

# A Solar System Test of Mach's Principle with Gravimetric Data

Alexander Unzicker

Pestalozzi-Gymnasium München, Germany

aunzicker@lrz.uni-muenchen.de

Karl Fabian

Norwegian Geological Survey Trondheim, Norway

karl.fabian@ngu.no

October 7th, 2006

## Abstract

We present a new test for a possible Mach-Sciama dependence of the Gravitational constant  $G$ . According to Ernst Mach (1838-1916), the gravitational interaction depends on the distribution of masses in the universe. A corresponding hypothesis of Sciama (1953) on the gravitational constant,  $c^2/G = \sum m_i/r_i$ , can be tested since the elliptic earth orbit should then cause minute annual variations in  $G$ . The test is performed by analyzing the gravity signals of a network of superconducting gravimeters (SG) which reach a precision of  $10^{-10} m/s^2$ . After reducing the signal by modelling tidal, meteorologic and geophysical effects, no significant evidence for the above dependence is found.

## 1 Introduction

Ernst Mach (1838-1916) suggested that the origin of gravitational interaction could depend on the presence of all masses in the universe. After the availability of cosmological data in the 1930s, the approximate coincidence  $\frac{c^2}{G} = \frac{m_u}{r_u}$  (where  $m_u, r_u$  refers to mass and radius of the universe) observed by Dirac (1938) pushed the development of that principle. However, despite its fascinating implications, very few quantitative statements of Mach's principle have been developed yet. Sciama (1953) deduced by a gravitomagnetic analogy a theory in which a dependence of the gravitational constant on the mass distribution of the universe,

$$\frac{c^2}{G} = \sum \frac{m_i}{r_i}, \quad (1)$$

is proposed. He estimated the respective contributions of the solar system, the galaxy, and the extragalactic matter, found the latter to be greatly dom-

inant and concluded that the coupling  $G$  is 'practically constant over the distances and times available to observation'. Since

$$\frac{M_S}{1AU} \frac{c^2}{G} \approx 10^{-8}, \quad (2)$$

the elliptic earth orbit (eccentricity  $\epsilon = 0.0167$ ) with an oscillating distance to the sun leads to a spatiotemporal variation the above sum (1). If such a variation of  $G$  were true, the effect on local gravity measurements of  $g$  would be about  $1.64 nm/s^2$ , which can be approached by modern superconducting gravimeters (SG). There are already hints that the hypothesis (1) is unlikely. For example, the Hubble expansion should cause a drift in  $G$  that exceeds the present observational evidence<sup>1</sup> for  $\frac{\dot{G}}{G} < 10^{-12} yr^{-1}$ . However, all these tests rely on cosmological models, whereas the test described here uses just celestial mechanics data. Moreover, it is sensitive to a annual oscillation of  $G$  on earth and there-

<sup>1</sup>See Uzan (2003) for an overview.

fore to a spatial variation of  $G$  rather to a drift, which is usually predicted by the Hubble expansion.

Though superconducting gravimeters (SG) have an extraordinary precision, unfortunately a variety of effects practically masks the detection of a possible signal of the described type. SG time series have been analyzed recently (Amalvict et. al. 2004; Kroner, Jahr, and Jentsch 2004; Boy and Hinderer 2004; Harnisch and Harnisch 2006), reducing the raw data with an appropriate modelling of known effects. Due to difficulties, the results regarding the long-term signal of the reduced data (gravity residuals) are not yet coherent.

The dominant signal of the direct solar and lunar tides can be eliminated relatively easily. The tidal attraction creates then a deformation of the earth which still can be modelled, though elastic properties of the earth enter here. Considerably more difficult is the calculation of the deformation of the earth crust due to the tidal shift of oceanic water masses (ocean loading).

Besides these phenomena which occur at well-known frequencies, meteorologic effects influence the gravity signal. Obviously, air masses above the SG reduce surface gravity, thus an anticorrelation with pressure is observed. Again, besides the direct effect, the air mass loading creates a deformation of the crust which is relevant. Independently of the pressure, cold air masses, being closer to the SG, have a slightly stronger effect on the signal; thus temperature data are needed as well. Groundwater level variations show a significant influence on the data, too. Very interesting is the extraction of the polar motion signal. Since  $g$  varies with latitude  $\varphi$ , a shift of the rotation axis of the earth effectively changes  $\varphi$  and therefore the locally measured  $g$ .

## 2 Data analysis and reduction by modelling

### 2.1 General method

Our data analysis consists in three steps. After eliminating errors and offsets, in a second step we try to model all physical effects that influence the gravity signal by avoiding any fitting parameters, trying to avoid misinterpretation of the remaining residual. In a third step, physical parameters like the gravimetric factor for polar motion are introduced in a

least-square-fitting routine and spectral filtering is performed where appropriate.

### 2.2 Raw data preparation

The raw gravity data are public available at the web site of the global geodynamics project (GGP) [ggp.gfz-potsdam.de](http://ggp.gfz-potsdam.de) (ask for a guest account). Whenever possible, we used the so-called ‘corrected minute data’ \*22.ggp instead of the ‘minute data’. According to the description, gaps due to instrument maintenance are filled with synthetic signal and offsets are adjusted. There are remaining gaps and offsets however; we corrected the latter ones by estimating the ‘jumps’ after data reduction described below, then redoing the automatized analysis. Since our interest was the long-term-signal, the minute data were filtered and averaged in a first step to 10 mins. Gaps and corrupted signal was labelled in order to take it out from the final analysis. Pressure data were prepared accordingly; in the few cases where absolute pressure information was missing, it was estimated from mean barometric pressure of the station height.<sup>2</sup>

### 2.3 Tidal effects

Most of the tidal analysis is nowadays done by software packages (e.g. Wenzel 1996) that determine factors and phases for a variety of spectral components. They are based on the tidal potential computed by Hartmann and Wenzel (1995). To separate different physical mechanisms, we found it interesting instead to use just the public available data of planetary motion.

**Direct attraction.** NASA provides on their ‘HORIZONS’- website<sup>3</sup> the most precise ephemeris data, available, DE 405, which is continuously updated with recent space mission results. Since the other planets are negligible for our purposes, we used hourly ephemeris data of moon and sun in the geocentric<sup>4</sup> coordinate system of equinox 2000, and did a 3D-spline interpolation to 10 mins. Since the position of the SG station can be computed from the hour angle and the station height and latitude

<sup>2</sup>For linear regression analysis done by many groups, the absolute pressure value is indeed obsolete.

<sup>3</sup><http://ssd.jpl.nasa.gov/?horizons>

<sup>4</sup>Otherwise, one had to deal with earth precession etc.

(using an ellipsoidal earth model), the vectorial difference of the gravitational force acting on the earth barycenter and on the station can be computed easily. Since this difference is in general not perpendicular to the earth surface, scalar multiplication with the station normal vector  $\vec{n}$  antiparallel to  $\vec{g}$  is performed. Since SG instruments automatically adjust themselves into the direction of  $\vec{g}$ , a correction for the centrifugal force is added to the geometric component of  $\vec{n}$  computed from latitude. For illustration, fig. (1) shows the solar component of this direct tide for one year. The seasonal effect of azimuthal height and the ellipticity of the earth orbit (slightly changing top line) is nicely reflected.

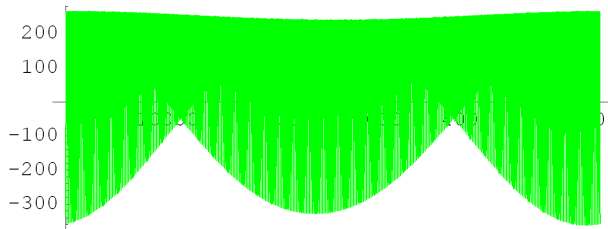


Figure 1: Direct solar tide effect for the Moxa station, 2001.

Accordingly, fig. (2) shows the solar and lunar component and its sum for one month (June 2001) computed for the Moxa station.

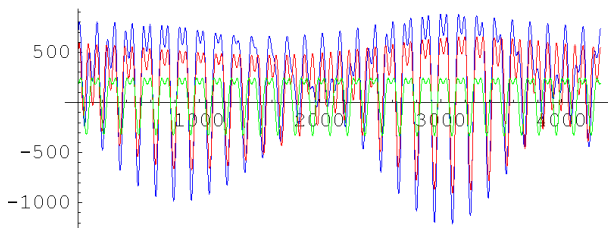


Figure 2: Direct solar (green) and lunar (red) tides and their sum (blue) for June 2001 in Moxa.

Comparison to the gravity signal from the GGP site, fig. (3), shows that the direct tidal effect is by far the dominant part of the SG signal. exemplarily depicted for the Moxa station, June 2001.

**Earth deformation tides.** Besides the direct effect, the earth as a deformable body responds elastically to the direct tide. Instead of determining the

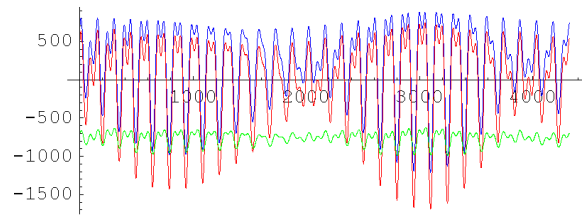


Figure 3: Gravity signal (red), direct tide computed from ephemeris data (blue), and the difference (green) for June 2001 of the Moxa station.

a priori unknown elastic constants of the earth by fitting, as a first approximation we calculate the deformation by analogy to the well-known deformation the earth undergoes as a reaction to its rotation. Assuming linear elasticity<sup>5</sup>, a stretch in the equatorial plane induced by the centrifugal force is equivalent to a squeeze along the pole axis with the doubled force.<sup>6</sup> Instead of squeezing, a gravitation celestial body stretches the earth along the visual axis to the body, causing thus a prolate deformation instead of the oblate one coming from the earth rotation. To compute the gravity effect, we can simply use the international gravity formula for latitude  $\lambda$ <sup>7</sup>

$$g(\lambda) := g_0 \frac{(1 + k_0 \sin(\lambda)^2)}{\sqrt{1 - e_2 \sin(\lambda)^2}}; \quad (3)$$

with  $g_0 = 9.7803267714$ ,  $k_0 = 0.00193185138639$  and  $e_2 = 0.00669437999013$ , and subtract the centrifugal term

$$g_k(\lambda) = g(\lambda) - a_z(\lambda). \quad (4)$$

If we take the spherical average of  $g_k(\lambda)$ ,

$$g_0 = \frac{1}{2\pi} \int_0^{\pi} \cos(\lambda) g_k(\lambda) d\lambda \quad (5)$$

$\bar{g}_k(\lambda) := g_k(\lambda) - g_0$  describes the gravity due to the oblate deformation only. If  $f_t$  is the maximal tidal force performed by the celestial body along the visual axis, then the gravity effect due to the corresponding prolate deformation computes as

$$\frac{f_t}{2a_z(0)} \bar{g}_k(\lambda), \quad (6)$$

<sup>5</sup>which is justified since we have geometrically small deviations from the sphere shape

<sup>6</sup>The stretching force acts in two dimensions, the squeezing force in one.

<sup>7</sup>Numerical values from IUUG.

whereby  $\lambda$  now stands for the deviation angle from the visible axis.  $\lambda$  can again be computed for the SG station at any time. As as fig. (4) shows, the deformation tide is again the dominant part of the signal remaining in fig. (3). However, the simplified elasticity approach does not take into account that the centrifugal force, acting for billions of years, creates much more elastoplastic deformation than the tidal forces which act for hours only. The above calculation exaggerates therefore the true deformation by about 15%. Taking this into account and implementing the well-known phase shift of 3 deg of the deformation tide, a slightly better reduction of the signal is obtained, as fig. (5) shows.

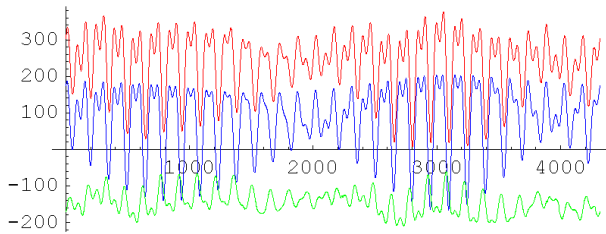


Figure 4: Residual of fig.(3) (red), deformation tide computed from prolate deformation (blue), and the remaining difference (green) for June 2001 of the Moxa station.

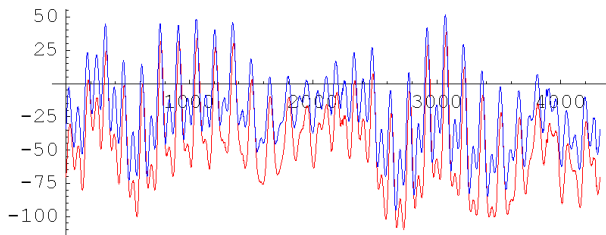


Figure 5: With a phase lag of 3 deg and a estimated reduced value 0.85 for the deformation tide, the residual of fig.(4) (red) is slightly improved (blue).

**Residual tide signal.** Despite the improvement in fig. (5) there is a clear residual signal at tidal frequencies. The main reason for it is the tidal shift of oceanic water masses which is not in phase with the deformation tide and which is greatly influenced by the distribution of land masses (ocean loading). Naturally, stations near the coast are more affected.

Typical amplitudes range from 10 to 100  $\frac{nm}{s^2}$ . There are several models that calculate tidal frequency components for a given location.<sup>8</sup> Since our focus of interest are long-term-effects rather than evaluating ocean loading models, we preferred to eliminate the remaining tidal signal by spectral filtering.

## 2.4 Meteorologic effects

**Pressure reduction.** Precise surface pressure data for the station location are provided by the GGP web site (same \*.ggp file). To give a first approximate correction, we calculated the attraction of an cylindrical air mass of radius 300 km (typical size of atmospheric disturbances) and 11 km height, using an isothermal barometric pressure formula with an estimated temperature for the station and taking the station pressure as overall surface pressure. A correction for the earth curvature was applied, too. The result is a clear improvement of the residual signal, see fig. (6). Amplitudes for the pressure effect can reach 50  $\frac{nm}{s^2}$ .

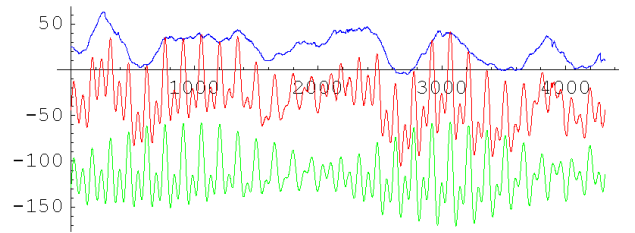


Figure 6: Residual signal from fig.(5) (red), pressure correction (blue) and the remaining difference. The residual still contains tidal frequencies due to ocean loading.

**Temperature effect.** A cold air mass, being closer to the SG, performs a greater gravitational attraction than a warm one, even if there is the same surface pressure. This is much more difficult to model, and even if temperature recordings of the stations were desirable, they could not be useful to the same extent, since temperature shows a greater local variability than pressure. Therefore, weather data for the region surrounding the SG station are

<sup>8</sup>Online calculation provided by H.-G. Scherneck, <http://www.oso.chalmers.se/loading/>.

needed. We used the freely available NCEP Reanalysis data<sup>9</sup> at the web site <http://www.cdc.noaa.gov/>, which provides on a 2.5 deg-grid four times daily humidity, temperature and geopotential height data for 17 pressure levels. For simplicity, we chose a 20 deg x 20 deg-grid centered around the SG station and considered all 17 pressure levels, since for appropriate modelling 3-dimensional data are needed (Neumeyer et. al. 2004). Thus even for the stations closest to the poles a distance of about 500 km to the station is covered. To summarize, for every station location there are  $9 \times 9 \times 17 = 1377$  data points. Every point is at the center of a cuboid which is assumed to have homogeneous density. To save computation time, the gravitational effect of every cuboid is first integrated analytically for every station, and the resulting weights are then multiplied with the time-dependent density. Since density data are not provided, the geopotential height for the pressure level,  $h(p)$ , is by vertical interpolation transformed into a function  $p(h)$ . Numerical differentiation yields with  $\rho = \frac{1}{g} \frac{dp}{dz}$  the density  $\rho(h)$ . This procedure turned out to be much more efficient and precise than using temperature data and the general equation of state  $pV = NKT$  and  $\rho = \frac{p}{kTm}$ , where  $k$  is the Boltzmann constant and  $m$  the molecular mass. Once the gravitational effect of the surrounding air masses is computed as described above, the 6h-time series can be interpolated to 10 mins. Two problems however arise. The station pressure data is not only available more frequently, but also much more precise. Thus the loss in accuracy due to the inevitably less precise NCEP data could spoil the better physical modelling. We computed therefore an artificial reference pressure  $p_{Ncep}$  from the layer model above the station, and set the gravity correction  $g_{Ncep}$  in relation to the true station pressure  $p_{Station}$ , thus yielding the final correction

$$g_{final} = g_{Ncep} \frac{p_{Station}}{p_{Ncep}}. \quad (7)$$

Due to temporal interpolation there is still some high frequency noise introduced by this procedure, but the gain in accuracy for the long-term seasonal signal is considerably, as fig. (??) exemplarily shows for the Moxa station. During winter season, the upward air attraction is higher and therefore the signal lower.

<sup>9</sup>The \*.nc files were converted into ASCII-readable files by the freely available programm ncdump.exe.

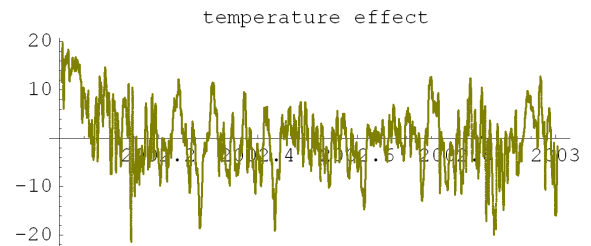


Figure 7: Difference between 3D atmospheric density calculation and pure station pressure correction for the SG in Moxa (Ger) for the year 2002. Summer and Winter are clearly distinguishable.

The temperature effect can reach as much as  $10 \frac{nm}{s^2}$ , with an average annual amplitude up to  $5 \frac{nm}{s^2}$ .

**Air mass loading.** The pressure distribution on earth creates a deformation of the crust that again manifests as a gravity change. A method for the calculation with Greens functions is presented in Neumeyer et. al. (2004). Since our global surface pressure data is much less precise than the station pressure, we restrict here to a linear regression to the station pressure, since the loading effect is strongly correlated to it. Air mass loading can cause effects up to  $10 \frac{nm}{s^2}$ .

**Hydrology.** Ground water level variations can have considerable influence on the SG signal, although a correlation as well as an anticorrelation may occur, depending on the station location being above (e.g. Sutherland) or below (e.g. Moxa) the surrounding terrain. However, groundwater and rainfall data are provided by some stations only. After correcting gaps due to malfunction, we determined the correlation by least-square fitting, since detailed geological information about rock porosity etc. is usually missing. Hydrologic effects are highly station-dependent and may reach  $50 \frac{nm}{s^2}$  in extreme cases.

## 2.5 Geodynamic signals.

The rotation axis of the earth does not always point through the same point but shows an oscillation with an amplitude of some tens of meters (polar motion). Such a shift effectively changes the latitude of the SG station, and consequently, one expects

a change in the centrifugal force that has usually a component perpendicular to the station surface. This expected change is amplified by the so called gravimetric factor  $\delta$  (Loyer, Hinderer, and Boy 1999; Ducarme et. al. 2004), since a change in latitude causes a variation of  $g$  independently from the centrifugal force (see the above discussion on the international gravity formula).

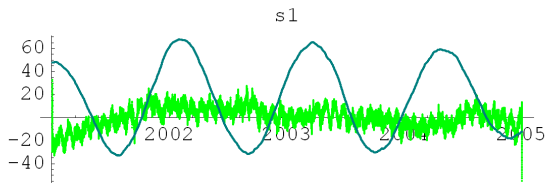


Figure 8: Example for polar motion signal (dark green) and residual signal after fitting for Sutherland, 2001-2004.

Due to VLBI techniques, very precise data are provided by the International Earth Orientation Service ([www.IERS.org](http://www.IERS.org)). It is easy to compute the effective change in latitude for the SG station and the expected form of the signal. We then determined the gravimetric  $\Delta$  factor by fitting. It is possible that  $\delta$  varies slightly with position. We do not know however any physical reason why  $\delta$  should vary considerably between the Chandler frequency (432 d) and the annual one (365.25 d). Fitting is done therefore with respect to the complete signal, not to separate frequencies.

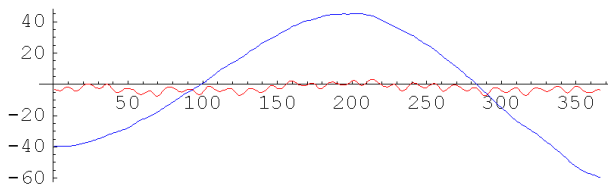


Figure 9: Predicted gravity changes due to length-of-day-variations (red, 10 times exaggerated), and polar motion signal, for Moxa, 2001.

**Length-of-day variations (LOD).** Variations of the length of the day and therefore of the rotational frequency  $\omega$  cause variations of the centrifugal force. Though this is in the range below  $2 \frac{nm}{s^2}$ , we included the LOD data in our analysis.

## 2.6 Drift.

All SG instruments show a drift that is not fully understood yet, thus absolute gravity measurements are not possible. The drift has to be eliminated by fitting a linear function in time.

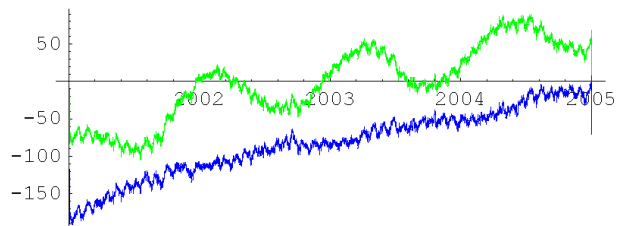


Figure 10: Signal with and without polar motion before removing the drift.

## 3 Results

### 3.1 Polar motion.

The polar motion signal is obtained after applying tide, pressure and temperature corrections and drift removal. For the plot fig. (11), tidal frequencies are filtered. The gravimetric factors  $\delta$  obtained by least-square fitting are shown in table 2.  $\delta = 1$ . would correspond to the centrifugal force change only, but the elastic response has to be taken into account, too. Our result agrees with Kroner et al. (2004) for Moxa, but  $\delta$  varies significantly with location. Contemporary fitting with pressure and temperature corrections does not change very much. Additional fitting to the groundwater level signal yields still lower values for  $\delta$ , 1.09 and 1.12 for Moxa and 1.02 and 1.03 for Sutherland (for Bolder and Canberra, no hydrologic data are available).

Station	temperature corr.	pressure only
Mo	1.10	1.13
Su	1.06	1.07
Bo	1.40	1.41
Cb	1.21	1.22

Table 1. Gravimetric factor  $\delta$  for different stations obtained

by fitting the polar motion signal, together with either the temperature correction (left) or the pressure correction only (right).

and Bolder has a stronger effect, whereas for the stations on the southern hemisphere the opposite effect is observed.

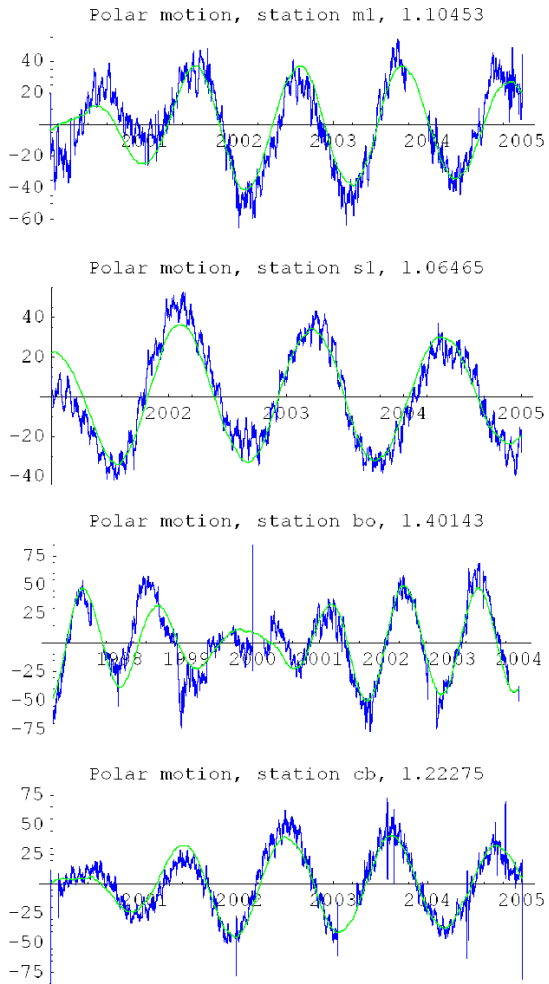


Figure 11: Polar motion signal after removing tides, pressure and temperature corrections, for the stations Moxa, Sutherland, Bolder, Canberra. The respective gravimetric factors obtained from fitting are shown in Table 1, left column.

### 3.2 Temperature corrections.

The 3D- density correction shows a clear annual signal resulting from different seasonal atmospheric densities. In Winter, the cold atmosphere over Moxa

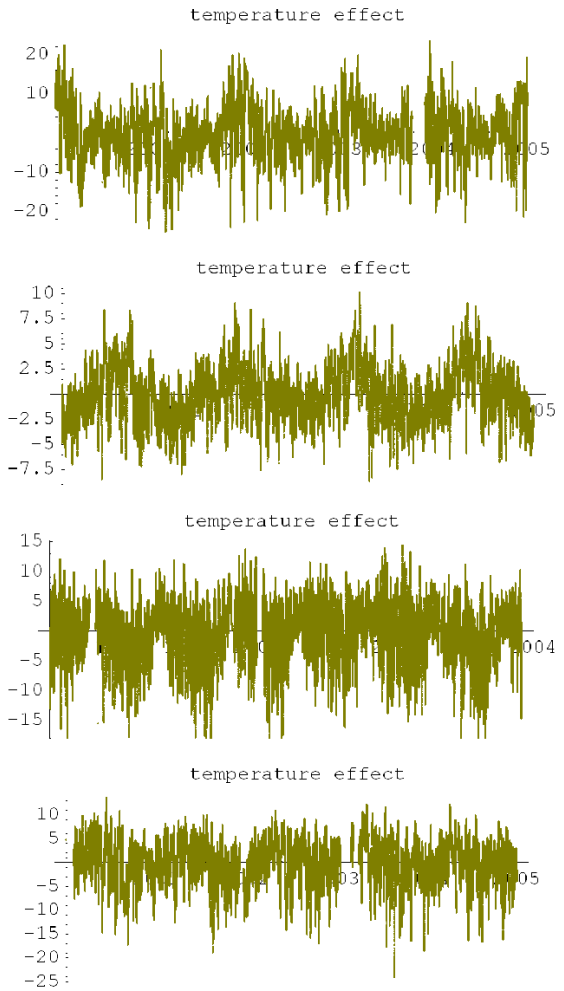


Figure 12: Difference between the simple pressure correction and the density correction in a 3D-model obtained from NCEP climate data, for the stations Moxa, Sutherland, Bolder, Canberra.

Since the temperature correction as described in section 2.4 introduces some high-frequency noise, the fitting quality is not improved (see Table 2).

Station	T	RMS	P	RMS
Mo	0.76	11.70	0.89	11.66
Su	0.81	10.36	1.00	10.32
Bo	0.75	16.12	0.93	16.13
Cb	0.70	26.99	0.84	27.0

Table 2.

‘TC’ stands for temperature correction, and ‘PR’ for pressure only. Due to insufficient temporal resolution of climate data, the high-frequency noise spoils the long-term improvement, as least-square deviations from the signal are concerned.

### 3.3 Machian signal

Since the possible Machian dependence has the same structure as it might be expected from other seasonal signals related to climate effects, there is considerable danger for misinterpretation. In particular, if such an influence is not modelled, the temperature-dependent atmospheric density may mimic a Machian signal *on the northern hemisphere*. Indeed, the respective stations show a high value in the middle column of table. 3 where temperature is not modelled. It is expected therefore that the temperature correction reduces the Machian factor, as it is observed for Moxa and Bolder. There is however a positive correlation with the Machian signal for Sutherland and Canberra, too, which cannot be a misinterpretation of climate seasons, since these effects should be reversed.

Since polar motion occurs at similar frequencies as well, a badly estimated  $\delta$  could be the reason for a fake Machian signal. With a  $\delta = 1.16$  fixed we find a positive correlation to the Machian signal as well, though with considerable variation.

Station	TC	PR	PF
Mo	2.49	3.43	1.13
Su	1.74	1.25	2.12
Bo	3.16	3.46	4.25
Cb	2.37	2.65	2.46

Table 3.

Fitting factor for the Mach-Sciama signal for the four stations under consideration. A factor 1. would indicate an annual signal of amplitude  $1.64 \frac{nm}{s^2}$  with a minimum at the perihelion (Dec). ‘TC’

stands for temperature correction, ‘PR’ for pressure only, and ‘PF’ for polar motion fixed. In the left and middle column, fitting is done contemporarily to atmospheric correction signal, the polar motion signal and the Mach-Sciama-signal. In the right column, polar motion is kept fixed to  $\delta = 1.16$ .

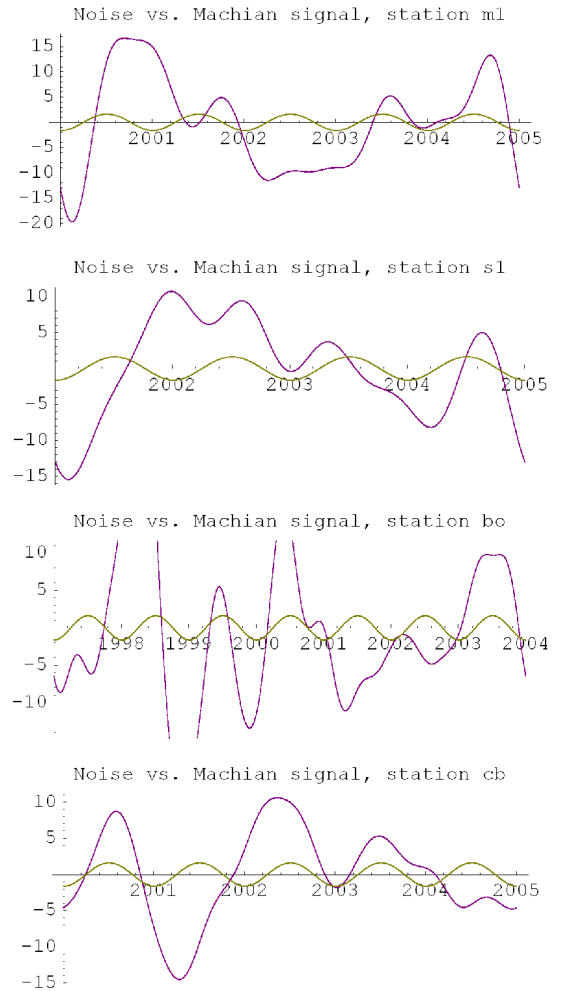


Figure 13: Residual signal after removing tides, pressure and temperature corrections, and polar motion, low-pass-filtered, for the stations Moxa, Sutherland, Bolder, Canberra

To put in evidence the difficulties in eliminating unwanted signals, fig. (13) shows the residual after applying corrections for tides, polar motion,

pressure and temperature. Additionally, since we are interested in the long-term components of the signal, all frequencies  $1/150d$  were cut off. The low-frequency noise due to unknown effects like station maintenance, instrument failures, insufficiently corrected gaps, drifts and offsets is still above the amplitude of the Machian signal,  $1.64 \frac{nm}{s^2}$ . Therefore we cannot attribute significant evidence to the fitting coefficients found above.

## 4 Discussion and Outlook

The large variation of the gravimetric factors for different locations has to be investigated further. While we do not see any reason why  $\delta$  should vary with frequency, local changes must be considered. Since polar motion is an effective change in latitude, gravity gradients having its origin in the mantle and core may cause such a variation.

We have shown how to analyze a possible Mach-Sciama-signal, in particular the comparison of the two hemispheres and climate modelling turns out to be important. Though we find a little signal with the correct sign for all stations, the overall noise is yet too large for attributing significance to it. A very unlikely hypothesis like the Mach-Sciama-dependence of  $G$  with its consequences for Newton's law needs much stronger evidence. Rather than refining the statistical analysis, we propose future efforts in improving the physical models. The found polar motion anomaly should be investigated first. To exclude climate effects, (possibly dry) SG stations on the southern hemisphere are desirable.

**Acknowledgement.** Gravity and pressure data are provided by the GGP network <http://ggp.gfz-potsdam.de>. NCEP climate reanalysis data are provided by the NOAA/OAR/ESRL PSD, Boulder, Colorado, USA, from their web site at <http://www.cdc.noaa.gov/>. Planetary ephemeris data is provided by NASA from the web site <http://ssd.jpl.nasa.gov/?horizons>. Earth orientation and LOD data are provided by <http://www.iers.org>. We are grateful to Corinna Kroner and to Thomas Klügel for helpful hints and suggestions.

## References

- Amalvict et. al. (2004). Long term and seasonal gravity changes at the strasburg station and their relation to crustal deformation and hydrology. *Journal of Geodynamics* 38, 343–353.
- Boy, J.-P. and J. Hinderer (2004). Study of the seasonal gravity signal in superconducting gravimeter data. *Journal of Geodynamics* 41, 227–233.
- Dirac, P. A. M. (1938). A new basis for cosmology. *Proc. Roy. Soc. London A* 165, 199–208.
- Ducarme et. al. (2004). Global analysis of the ggp gravimeters network for the estimation of the pole tide gravimetric amplitude factor. *Journal of Geodynamics* 41(334-344).
- Harnisch, M. and G. Harnisch (2006). Study of long-term gravity variations, based on data of the ggp gravity co-operation. *Journal of Geodynamics* 41(318-325).
- Hartmann, T. and H.-G. Wenzel (1995). The hw95 tidal potential catalogue. *Geophysics Research Letters* 22(24), 3553–3556.
- Kroner, C., T. Jahr, and G. Jentsch (2004). Results from 44 months of observations with asuperconducting gravimeter at moxa/germany. *Journal of Geodynamics* 38, 263–280.
- Loyer, S., J. Hinderer, and J.-P. Boy (1999). Determination of the gravimetric factor at the chandler period from earth orientation data and superconducting gravimeter observations. *Geophys. J. Int.* 126, 1–7.
- Neumeyer et. al. (2004). Gravity reduction with d-dimensional atmospheric pressure data for precise ground gravity measurements. *Journal of Geodynamics* 38, 437–450.
- Sciama, D. W. (1953). On the origin of inertia. *Monthly Notices of the Royal Astronomical Society* 113, 34–42.
- Uzan, J.-P. (2003). The fundamental constants and their variation: observational and theoretical status, hep-ph/0205340. *Reviews of modern physics* 75, 403–455.
- Wenzel, H.-G. (1996). The nanogal software: Earth tide processing package ETERNA 3.30. *Bull. d'Inf Marees Terr.* 124, 8425–9439.